THE FREE AND RESTRICTED DIFFUSION OF SILICON NANOCRYSTAL CLUSTERS

A Thesis
Submitted to the Graduate Faculty
of the
North Dakota State University
of Agriculture and Applied Science

By

Ahmed Bahgat Elbaradei

In Partial Fulfillment of the Requirements
for the Degree of
MASTER OF SCIENCE

Major Program:
Materials and Nanotechnology

June 2015

Fargo, North Dakota

North Dakota State University
Graduate School

Title

The Free And Restricted Diffusion Of Silicon Nanocrystal Clusters

By

Ahmed Bahgat Elbaradei

The Supervisory Committee certifies that this ***disquisition*** complies with North Dakota State University's regulations and meets the accepted standards for the degree of

MASTER OF SCIENCE

SUPERVISORY COMMITTEE:

Erik Hobbie
Chair

Orven Swenson

Andrew Croll

Approved:

6/16/2015	Erik Hobbie
Date	Department Chair

ABSTRACT

Biological applications for silicon nanocrystals (SiNCs) have recently gained more attention because of silicon's low toxicity. But, to be able to use SiNCs in applications such as biological sensors, labeling or drug delivery we need to understand their transport in different environments and their interaction with cell membrane. I will review some different methods for the synthesis of, and I will give an accounting of encapsulating SiNCs with PEGylated phospholipids to make them soluble in water. I also studied the free diffusion of these micelles in water, as well as their restricted diffusion and interaction with giant unilamellar vesicles (GUVs). I studied their restricted diffusion in oil emulsions. I was able to calculate the diffusion coefficient for a large number of micelles moving freely in water. I also measured the effect of water on the SiNC micelles intensity and observed the difference between the restricted diffusion in liposomes and emulsions.

ACKNOWLEDGMENTS

I owe the success of this work to Erik Hobbie. He was so supportive, helpful and always understanding. At the very beginning when I joined the Materials and Nanotechnology program, I didn't have much knowledge about silicon nanomaterials and their applications. There was much to learn and Erik always had his door open for me. I have to mention that he deserves a lot of credits for his patience and his understanding while I became more proficient in English as well. I was always working on weekends and I always bothered Erik with my emails on Friday, and surprisingly he was answering immediately and passionately to figure out the issue. Erik is my idol for hard work and motivation. I also appreciate his support through the recent period of challenge in my personal life.

My companion in research was a guy who I will always look up to as a nice, smart, hard-working and tall guy; Joseph Miller, or I should say Dr. Joey the fastidious. Joe and I worked a lot together on many projects and I wish I could go back in time to appreciate his fellowship more and to learn from him. We worked on measuring quantum yield by using an integrating sphere for a long time until we called ourselves quantum yield warriors. We also worked on several projects together, which helped me get closer to him and he was always there to offer advice and instruction, besides being fastidious. Samuel Brown (or as I like to call him Sam-Yol. I don't think he likes it but this was how I teased him) is a very hard worker who made me feel guilty about my own work ethic on occasion. We took many courses together and he was the best company I could ever ask for. Mr. Matthew Semler (*maestro de los osos*, or master of the bears) and I had a lot of discussions together and he was always a good listener and I really enjoyed our daily chats, even though I often

felt a bit guilty for wasting his time. Damith Rozario was eating Greek yogurt all the time and I would never forgive him. I was always successful in getting him scared very easily but he was always there for me. Bekele Gurmessa was always giving me advice and I was listening to him for motivation. John Harris and I took courses together and he was always helpful so that I was not feeling alone in the hardships of physics courses. I really want to thank all my colleagues in the lab because what I learned from them is priceless. I also want to thank Xinann Wang for supporting me through hard times, as well as Orven Swenson and Andrew Croll for being a part of my committee and supporting me. I want to thank all my friends and professors in the physics department; Deyan Mihaylov, Goetz Kaehler, Nathaniel Grosz and Paul Omernik. We had a lot of discussions while we were working on homework. I also can't forget to acknowledge Patty or Patricia Hartsoch who was a great support. Thank you all for being part of my journey and experience.

DEDICATION

To Dad, who dedicated his life to us.

Mom, who was always believing in me.My brother, who taught me a lot of stuff in this world.

My sister, who is my best friend.

My love . . . . .

To both the Egyptian and Tunisian revolutions.

To all my friends who I got across them through my journey. Thank YOU

TABLE OF CONTENTS

LIST OF FIGURES

CHAPTER 1. INTRODUCTION

Semiconductors are now widely used in microelectronic circuits and in optoelectronic devices such as light-emitting diodes, photovoltaic devices, and light detectors, etc.[1] Semiconductor materials are characterized by band gaps between 0.5 and 3 eV, which makes them ideal materials for many electronic and optical applications. The ability to control a semiconductors band gap could open the door to many new applications. Semiconductor nanocrystals give us this ability to change and control the band gap compared to the bulk semiconductors. We can change the semiconductors energy gap over quite a wide range based on a mechanism known as quantum confinement. Quantum dots (QDs) are very tiny particles on the order of a nanometer in size. They are composed of a hundred to a thousand atoms comprised from an element, such as silicon or germanium, or a compound, such as CdS or CdSe.

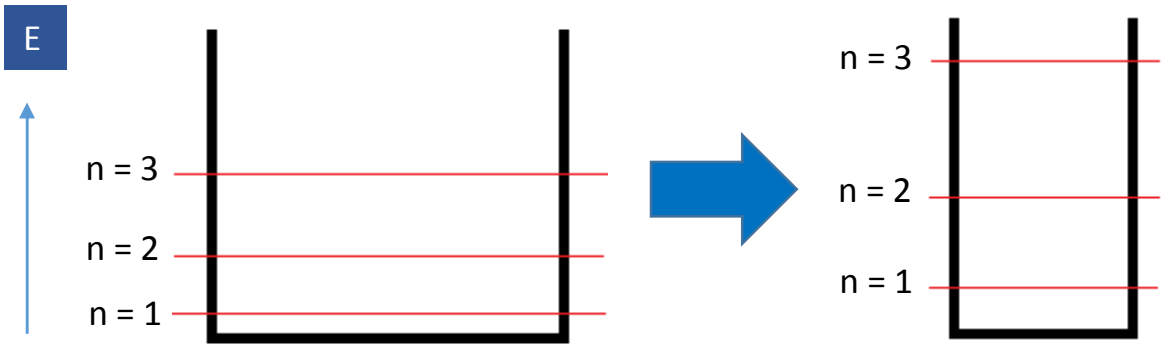

Figure 1: Schematic for a particle in a box and the quantum confinement effect.

Solving Schrodinger's equation for a particle in a box gives equation (1.1), which is showing that the energy gap is inversely proportional with the radius of the dot squared (Figure 1). So, we can control the energy gap by changing the size of the quantum dot.

$$E_n = \frac{n^2 h^2}{8mL^2} \tag{1.1}$$

Through the process of photoluminescence, a change of the energy gap changes the wavelength of the light emitted. Size-tunable material properties are typically found when the so-called Bohr exciton radius is larger than the physical size of the semiconductor material. They are typically characterized by bandgaps between 0.5 and 3 eV, which makes them ideal materials for many electronic and optical applications.[1, 2]

Nanomaterials have tremendous potential in biological applications and drug delivery. Cd-based QDs have been used in the targeted *in-vivo* imaging of tumors. However, Cd poses problems because of the potential toxicity at low concentration, with recent studies indicating that cadmium-ion release is a major concern.[3] One solution is to apply a biocompatible coating to the core, which has been shown to decrease the cytotoxicity of these QDs. Beyond this approach, new heavy-metal free QDs are needed for *in vivo* applications. Silicon is nontoxic in its elemental form compared to group II-VI and IV-VI QDs. Si-QDs were claimed to be at least 10 times safer than Cd-based QDs under UV irradiation.[3] One of the major obstacles for applications of silicon nanocrystals, however, is oxidative degradation in the biological environment. Studies have shown that surface functionalization and PEGylated-micelle encapsulation of Si-QDs can overcome this problem.[4]

Although silicon nanocrystals (SiNCs) are gaining more attention, their transport and interaction with cell membranes is not well understood. To be able to study their diffusion inside cells, we studied their free diffusion first and then studied their diffusion inside artificial cells; giant bilayer liposomes. There are many synthesis methods available for silicon nanocrystals. Non-thermal plasma synthesis is the method used to create the

SiNCs that we used here. In Chapter 2, we explained in detail the different synthesis methods. To be able to study SiNC diffusion in water, however, we first need to make them soluble in water. To do so, we encapsulated the SiNCs with PEGylated phospholipids, which surround the QDs and make them water-soluble. Next, we recorded videos under photoluminescent observation for the free diffusion of these micelles, and using a Matlab code we were able to track the particles trajectories and obtain their diffusion coefficients for further study. Optical measurements were generated using visible/NIR fluorescence imaging and an inverted Olympus microscope attached to Electronic Multiplied Charged Coupled Device (EMCCD). The next step was to prepare the giant unilamellar vesicles (GUVs) that mimic the structure of the cell membranes. We used the gentle hydration method to prepare them and introduce our micelles into the liposomes. We then recorded more videos for the restricted diffusion of these micelles inside the GUVs using the previous setup and then started analyzing this data using Matlab to obtain position *vs.* time data. Finally, we studied the restricted diffusion of the same SiNC micelles inside water-in-toluene emulsions. We explain the method we used to prepare the emulsions in details in Chapter 4. We recorded videos for micelle diffusion and were able to track the particles inside the emulsions and calculate the distance of the micelle from the interfaces and study the potential effect of the interface on the diffusion of the micelles near the boundary.

CHAPTER 2. NANOCRYSTAL SYNTHESIS

2.1. Chemical Etching

The most frequently used method for the preparation of porous silicon is the chemical etching or the electrochemical etching of silicon wafers. In this method, a silicon wafer is electrochemically polarized in an electrolyte containing hydrofluoric acid. The wafer dissolves slowly, forming cavities that percolate throughout the sample producing porous silicon. Removal of the formed nanocrystal can be done by sonication in a solvent bath or the material can be left intact for further study.[5]

2.2. Laser Ablation in Liquids (LAL)

Making silicon nanocrystals by laser ablation in liquids (LAL) requires a two-stage process. The first stage is the nanosecond laser ablation of a silicon target in chloroform, which induces the formation of large composite polycrystalline particles (20-100 nm). The second stage is the ultrasonic post treatment of the silicon nanoparticles (SiNPs) in the presence of HF, which disintegrates them and releases small individual nanocrystals (NCs).

A p-type cz-silicon wafer with a resistivity of **10-20 Ω** is typically ultrasonicated in deionized water and then ethanol for 1 hour. The wafer is then immersed in $CHCl_3$ and targeted by a pulsed Nd:YAG laser (355nm, 40ns pulse duration, 5 KHz repetition rate). Twenty scans is typically sufficient to see a brownish color in the liquid. After evaporating the chloroform, a post treatment for the precipitate is needed to obtain small size monocrystalline silicon nanoparticles. This post physicochemical treatment is achieved by exposure to isopropanol, HF and hexane (3:1:3) under continuous ultrasonication. Testing of these SiNPs by transmission electron microscopy (TEM) and by high resolution TEM

(HRTEM) at 100 and 200 kV coupled with Raman scattering measurements are used to confirm the size and crystallinity of the SiNCs.[6]

2.3. Solution Based

In the solution-based method, thermal decomposition of HSQ (hydrogen silsesquioxane) is achieved by heating under a flow of argon and hydrogen gas to a peak temperature of 1100-1400°C, depending on the desired nanocrystal size. The second step is to grind the brown/black glassy product into a brown powder with a grain size of 200 nm. HF and HCL are then used to etch the oxide to yield hydride-terminated SiNCs, which are then centrifuged to isolate the NCs from the HF. To reduce the impact of oxidization - which affects the photophysical properties of NCs - requires a passivation step, which is achieved by rinsing the light brown precipitate in ethanol and toluene and then dispersing it in 8 mL of 1-dodecene and 2 mL of 1-octadecene. The resulting cloudy brown dispersion is heated to 190 °C for 8 h, producing a clear dark-orange dispersion. After washing and dispersing in toluene, the concentrated nanocrystal dispersions are heated under vacuum for 24 h at 200 °C to remove the excess ligand. Finally, the nanocrystals are dispersed in toluene again for further study.[7]

2.4. Laser Pyrolysis

The laser pyrolysis method combines vapor-based and solution-phase process using inexpensive commodity chemicals to produce SiNPs at high rates (20-200 mg/h). CO_2 laser induced pyrolysis of silane produces particles with an average diameter of 5 nm. These SiNPs were prepared and later reduced by etching with mixtures of hydrofluoric acid (HF) and nitric acid (HNO_3). There are some problems associated with passivation so that these particles are not well dispersed in most solvents and do not have stable photoluminescence

(PL). The PL intensity tends to decay with time while the PL peak shifts. Surface functionalization was essential to produce particles with good properties. The surface functionalization has two approaches. The first is hydrosilylation of Si-H surfaces, and the second is silanization of Si-OH surfaces. Modifying the surface of the etched luminescent silicon nanoparticles allows the formation of a stable colloidal dispersion of these particles in different solvents.[8]

2.5. Ion Implantation

The ion implantation synthesis method requires a complex setup. A silicon ion source is accelerated through a fixed electrostatic potential towards a magnetic mass-spectrometer which filters undesired ion species. Second, uniform irradiation is introduced through a beam or scanning system that is contained in a special chamber. This special chamber is important to control essential parameters such as vacuum level, sample position and temperature. The ions will hit the sample substrate to a specific depth depending on their energy. The substrate used for producing SiQDs is often silicon dioxide. Once the ions reach the limit of supersaturation of the solid, they will nucleate SiNCs.[5]

2.6. Sol-Gel Pyrolysis

Enhancement of SiNC optical properties is important for applications and has been studied extensively. Some methods used for the synthesis of SiNCs can be expensive and the SiNCs produced have a broad size distribution and a low density. The sol-gel pyrolysis method uses tetraethylorathosilicate HSi (OCH_2CH_3) or $HSi(OR)_3$, which is commercially available. The first step is hydrolyzation with water for the hybrid silicon alkoxide, which substitutes the OR group with a silanol Si-OH group. The second step is condensation for the previous mixture to react to form a siloxane (Si-O-Si) bonded network. The last step is

pyrolysis at a temperature above 1000 °C where the Si-H moieties present react to H_2 and Si-Si bonds. The Si-Si bonds reorganize and form SiNCs.[5]

2.7. SiO_x/SiO_2 Stoichiometric Annealing

Forming precise nanometer-sized silicon crystals has always been a challenge. One of the first methods to control the size was a SiO/SiO_2 superlattice approach. The approach uses molecular beam epitaxy and UV-ozone oxidation to grow precise nanometer-sized amorphous silicon layers between SiO_2 layers. Thermal evaporation of SiO powder is done at 1000 °C under high vacuum. Oxygen is added through the growth process to control the stoichiometry. The next step is to anneal the layers at 1100 °C in a nitrogen atmosphere. Because of the instability of nonstoichiometric oxides such as SiO_x at high temperature, they decompose into the two stable components Si and SiO_2 [5]:

$$SiO_x \rightarrow \frac{x}{2} SiO_2 + \left(1 - \frac{x}{2}\right) Si. \quad (2.1)$$

2.8. Solution Method via Reverse Micelles

A one-pot synthesis was able to present an efficient method for fabricating colloidal SiQDs with a modifiable surface. Allyl trichlorosilane were used as a surfactant and reactant to surround self-assembling halogenated silane precursors (SiX_4, X= Cl, Br) in toluene as shown in figure 2. The trichlorosilane formed a reverse micelle around the SiX_4 core and then was treated with $LiAlH_4$ to yield SiQDs with alkene groups attached to the surface. Transmission electron microscopy (TEM), high resolution TEM (HRTEM) and quantum yield measurements have been used to characterize the SiQDs.[9]

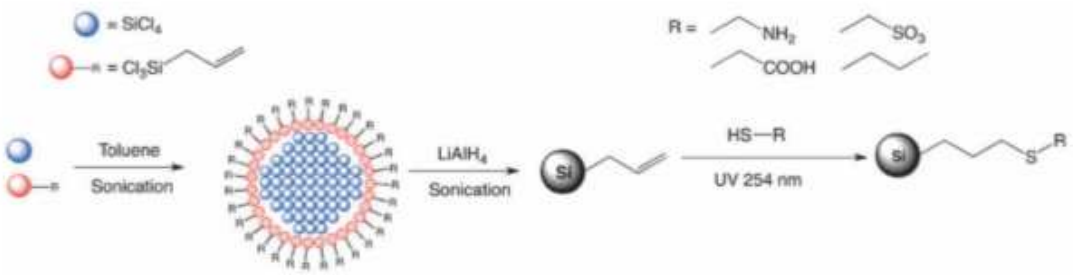

Figure 2: One-pot synthesis of alkene coated SiQDs and further functionalization via thiol-ene click chemistry.[9]

2.9. Low Pressure Non-thermal Plasma

The different states of matter generally found on earth are solid, liquid, and gas. Sir William Crookes, an English physicist, identified plasma in 1879. The word "plasma" was first applied to an ionized gas by Dr. Irving Langmuir, an American chemist and physicist, in 1929. A plasma consists of a collection of free moving electrons and ions - atoms that have lost electrons. Energy is needed to strip electrons from atoms to make a plasma. The energy can be of various origins: thermal, electrical, or light (ultraviolet light or intense visible light from a laser). With insufficient sustaining power, plasmas recombine into a neutral gas. A plasma can be accelerated and steered by electric and magnetic fields, which allows it to be controlled and applied. Plasma research is yielding a greater understanding of the universe. It also provides many practical uses: new manufacturing techniques, consumer products and the prospect of abundant energy, more efficient lighting, surface cleaning, waste removal, and many more application topics. Plasmas can be classified as “thermal” or “non-thermal” based on the temperature and thermal equilibrium between the electrons, ions and neutrals. In thermal plasmas, the electrons and gas temperature are in equilibrium with each other, like in the sun and lightning. In the non-thermal plasmas, the

electrons and gas temperatures are not in equilibrium with each other, like the aurora borealis.[10]

In its early years, this work was motivated by particle formation occurring as a contamination problem, both in semiconductor processing and in the manufacture of solar cells. Hence, the initial main thrust of studying particle formation in plasmas was to avoid the nucleation of particles.[11-13] The most important contribution of this method has been that nanocrystals can be generated at gas temperatures as low as room temperature and the approach has yielded silicon nanocrystals several tens of nanometers in size. Due to their size these nanoparticles have been investigated for electronic device applications in nanoparticle-based transistors.[5]

The main principle of plasma discharge is that when an electric field is applied to a gas under low pressure, electrons easily get accelerated to energies sufficient to electronically excite and ionize the surrounding gas atoms. In steady state, the ionization produced by energetic electrons will precisely balance the charge carrier losses through diffusion to the wall, recombination, and other processes.

Non-thermal plasmas are typically characterized by very hot electrons with temperatures between 20000-50000 K (~2-5 eV) and significantly colder positive ions and neutral molecules, whose temperatures are very effective in dissociating precursor gas molecules.[14, 15] They also lead to a buildup of electric field within the plasma wherever the plasma is in contact with boundaries such as reactor walls or the surfaces of nanoparticles. An interesting feature of the non-thermal plasma method is the selective ability of the temperature; the nanocrystals will be at several hundreds of Kelvin while the gas temperature will be much lower. This makes nonthermal plasmas attractive for the

synthesis of nanocrystals of covalently bonded semiconductors such as group IV and III-V semiconductors. Studies on silicon nanoparticles suggest that the crystallization temperature of particles with diameters of 4, 6, 8, and 10 nm are 773, 1073, 1173, and 1273 K respectively.[16] Thus, it is quite surprising that nanocystals requiring such high crystallization temperature are formed in plasmas at low gas temperature. In newer approaches they determined that the gas temperatures were between 420 and 520 K, which is significantly lower than the crystallization temperatures reported for small silicon nanoparticles. The only logical conclusion from this observation is that the nanoparticles in the plasma are at significantly higher temperatures than the surrounding gas.

The typical reactor consists of a quartz tube with 9.5 mm outer diameter and 6.8 mm inner diameter, mounted on a gas delivery line and exhaust system with ultratorr connectors as shown in Figure 2. Radiofrequency (RF) power is applied to the system using two ring electrodes.[17]

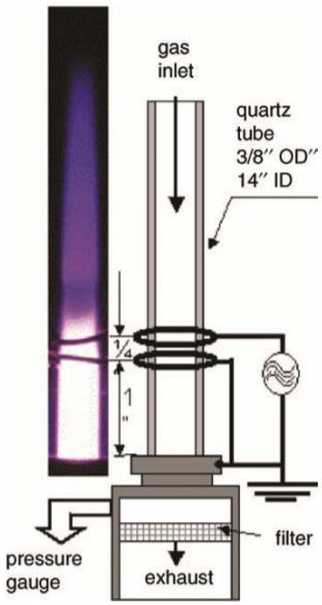

Figure 3: Schematic of a synthesis reactor with a digital image of the argon-silane plasma.[17]

The plasma is typically generated at a pressure of 187 Pa, but luminescent nanocrystals have also been obtained at pressures as high as 2000 Pa. Most of the experimental results presented were obtained at a pressure of 1.4 Torr since it was found that under these conditions the largest yield of nanocrystals could be achieved. Typical gas flow rates at 1.4 Torr are up to 100 sccm of Ar, around 15 sccm of SiH_4 (5 % dilution in either He or Ar), and a few sccm of additional hydrogen. The residence times of gas in the plasma, calculated on the basis of the gas flow velocity, are between a few tens of milliseconds to less than 5 ms. In figure (3), it can be seen that the plasma consists of two regions. In the part upstream of the electrodes, the plasma emission appears weaker than in the region downstream of the two electrodes. Also, significant growth of silicon film in the reactor tube can be observed upstream of the electrodes, while the growth is much less significant downstream of the ring electrodes. This suggests that very fast nucleation and precursor consumption occurs upstream of the electrodes.[17]

Plasma power plays a crucial role in this process. RF current and voltage have been measured to estimate the actual power consumption in the discharge, giving a value of 30 W. Given the very small discharge volume (2 cm^3), a considerable power density is achieved in the plasma region. A filter placed downstream of the discharge collects the particles produced in the plasma. The filter is made of a fine stainless steel mesh (400 wires/in.) and a few minutes of deposition are sufficient to completely coat the filter.[5]

2.10. Conclusion

We reviewed different methods used to produce SiNCs, touching on the advantages and disadvantages of each. The ultimate goal of these methods is to produce a broad range of sizes with stable and high-intensity photoluminescence at the lowest cost. In this work,

we used plasma-synthesized SiNCs because of their uniform size distribution and high quantum yield.

CHAPTER 3. PHOTOLUMINESCENCE PROPERTIES

Silicon nanocrystals (SiNCs) have many conceivable applications based on photoluminescence. To realize these applications, we require two photoluminescent properties; stability and efficiency. Stability in solution is important for dealing with colloidal silicon nanocrystals in different solvents. Also, silicon reacts with oxygen to form a silicon oxide layer, which affects the photoluminescence. Efficiency has important implications for determining the ability to use these SiNCs in different applications. This section will focus on the stability and efficiency of the SiNCs synthesized by the non-thermal plasma method. In our case, we are measuring the efficiency through the quantum yield; $QY = \frac{\#\ of\ photons\ emitted}{\#\ of\ photons\ absorbed}$. Measuring the QY allows us to evaluate how bright the photoluminescence (PL) will be. For drug delivery and biological applications, it is important that the SiNCs do not react with oxygen, so that they show a stable emission and a high quantum yield. The higher the quantum yield, the more opportunities will be available for different applications of SiNCs.

3.1. Stability

As we mentioned earlier, we need to produce stable SiNCs for different applications, and surface passivation is very effective for reducing the reaction of SiNCs with oxygen. A thermal liquid hydrosilylation reaction is the method used for the ligand passivation of the SiNCs, and using 1-dodecene as ligand for the passivation process allows SiNCs to be dispersed in most common organic solvents. Figure 4 illustrates the SiNC passivation process. The passivation process is always below 100% because of steric hindrance, and hence there will always be some dangling bonds. This incomplete passivation could allow oxygen to react with SiNCs. The reaction with oxygen can affect

the surface composition, changing the effective size with a blue shift that can reach 200 nm in the PL spectral emission.[18]

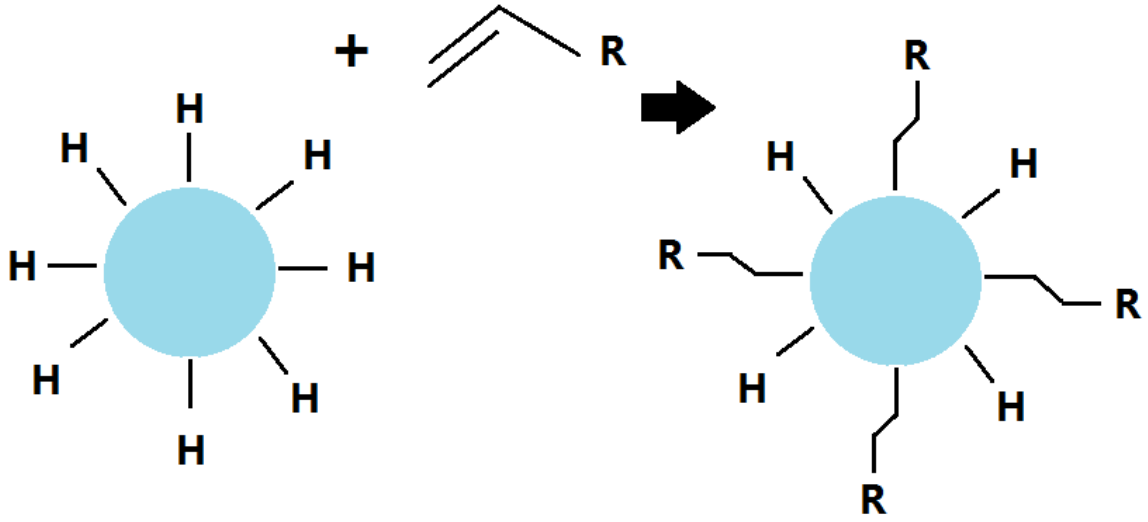

Figure 4: Illustration of a SiNC passivated with alken group (R) (octadecene, dodecene, and styrene).

3.2. Quantum Yield Measurement

The quantum yield of the plasma synthesized SiNCs used in this study was measured to be around 50 % immediately after synthesis.[19] Quantum yield is defined as the ratio of the number of photons that are emitted to the number of photons absorbed. To determine the QY of SiNCs we need to simultaneously record the absorption and emission spectra of a SiNC solution. To do this, we placed the solution in an integrating sphere, which was connected to an Ocean Optics QE65000 spectrometer through an optical fiber. We calibrated the spectrometer's spectral response with a calibration lamp; Ocean Optics halogen light source (HL-2000-CAL-ISP). A baseline was first collected for a vial containing pure solvent using an Omicron PhoxX® laser with wavelength of 375 nm. After subtraction of the reference baseline, the photoluminescence spectra of SiNCs dispersed in

hexane and sealed under a nitrogen atmosphere was collected. We take an average of three separate spectral measurements for both the sample and the reference. A typical PL after subtraction is shown in Figure 5. The QY value can be calculated by dividing the integrated of PL spectrum by the integrated absorption spectrum.

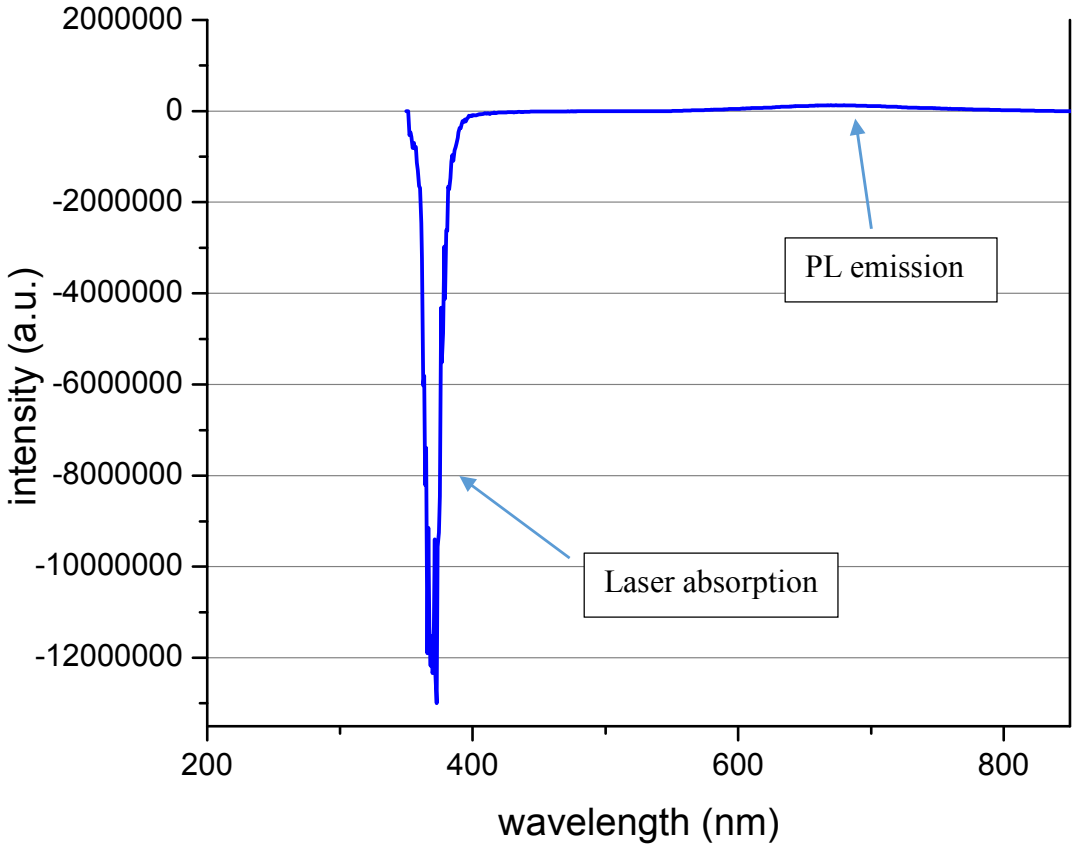

Figure 5: The Absorption and emission of a typical quantum yield measurement. The LED absorption is negative because of the background subtraction.

CHAPTER 4. FREE AND RESTRICTED DIFFUSION OF SiNCS

In this section, I report on the diffusion of the silicon nanocrystals (SiNCs) in different environments. First, I will give details about the theoretical basis of our experiments to study the diffusion of the micelles in different environments.

We studied the diffusion of micelles and nanocomposite particles in three different environments: free in water, confined inside giant unilamillar vesicles (GUVs), and inside water/toluene emulsions. First, I will report on the methods we used to make the SiNCs soluble in water by encapsulating them with PEGylated phospholipids. Second, I will report on the method we used to make GUVs. Third, I will report the experimental procedures we used to make the W/O emulsion. And finally, I will report on what we found by studying the micelle diffusion in these different environments.

4.1. Theoretical Background

Dropping a solid sphere in a fluid will make it accelerate until the drag force balances the gravitational force and the sphere reaches terminal velocity. This drag force is given by the following equation known as Stokes' law[20]:

$$F_s = 6\pi\eta R v. \tag{4.1}$$

The gravitational force is given by the equation:

$$F_g = \frac{4}{3}\,\pi\, R^3\, \Delta\rho\, g. \tag{4.2}$$

When force balance happens, both equations will equal each other and the sphere will reach a terminal velocity v_t:

$$v_t = \frac{2\, a^2 \Delta\rho\, g}{9\,\eta} \tag{4.3}$$

Combining Stokes' law and the Einstein equation will help us to understand the diffusion of such particles. Observing a spherical polymer colloid with an optical microscope shows that such particles move continuously in a random manner. This motion is termed Brownian motion after Robert Brown, a botanist, who observed the same phenomenon for plant pollen in 1827. Brownian motion results from collisions between the molecules of the fluid and the colloidal particles. In such a random walk, the mean square displacement is proportional to the number of steps and thus the time:

$$\langle \vec{r}(t) \rangle^2 = \alpha\, t. \tag{4.4}$$

Where, $\vec{r}(t)$ is the displacement vector after time t and α is a constant. The equation of motion can be written as:

$$m\frac{d^2\vec{r}}{dt^2} + \xi\,\frac{d\vec{r}}{dt} = \vec{F}_{random}. \tag{4.5}$$

Here, it is assumed that there is a drag force on the particle proportional to the velocity, with a drag coefficient ξ. For a sphere of radius a in a liquid of viscosity η, this is given by Stokes' law:

$$\xi = 6\pi\eta R. \tag{4.6}$$

Furthermore, with $r^2 = x^2 + y^2 + z^2 = 3\,x^2$, we can write $d(x^2)/dt = 2\,x(dx/dt)$, so multiplying equation (4.5) by x and rearranging yields:

$$\frac{\xi}{2}\frac{d(x^2)}{dt} = x\,F_{random} - mx\frac{d^2x}{dt^2}. \tag{4.7}$$

With:

$$x\frac{d^2x}{dt^2} = \frac{d}{dt}\left(x\frac{dx}{dt}\right) - \left(\frac{dx}{dt}\right)^2. \tag{4.8}$$

we get

$$\frac{\xi}{2}\frac{d\langle(x^2)\rangle}{dt} = \langle x\, F_{random}\rangle - m\frac{d}{dt}\langle x\,\frac{dx}{dt}\rangle - m\langle\left(\frac{dx}{dt}\right)^2\rangle. \tag{4.9}$$

The first and second term on the right hand side will time average to 0 because the direction of the random force and the velocity are random and uncorrelated with the position. So the equation becomes:

$$\frac{d\langle(x^2)\rangle}{dt} = 2\frac{kT}{\xi}. \tag{4.10}$$

and the total mean square displacement will be given by the following equation:

$$\langle(r)^2\rangle = \frac{6\,kT}{\xi}\,t. \tag{4.11}$$

Using the Einstein Formula

$$D = \frac{kT}{\xi}. \tag{4.12}$$

We get what is called the Stokes-Einstein equation:

$$D_{SE} = \frac{kT}{6\pi\eta R_h}. \tag{4.13}$$

This previous equation gives the diffusion coefficient of a colloid in a fluid and is the one we use to determine the radius of the micelles. Combining Equations (4.11) and (4.12) gives the diffusion coefficient as a function of mean square displacement in three dimensions [20]:

$$D = \frac{\langle (r)^2 \rangle}{6t}. \tag{4.14}$$

In our setup we apply the previous equation to determine the diffusion coefficient but projected to two dimensions as follows:

$$D = \frac{\langle (r)^2 \rangle}{4t}. \tag{4.15}$$

4.2. Experimental Procedures

4.2.1. Free Diffusion of Micelles

Preliminary experiments have recently been performed to understand the use of monodisperse, stable SiNCs for biological applications. To achieve that, we need to perform surface passivation to allow SiNCs to be stable in aqueous environments. We used polyethylene glycol (PEG) grafted phospholipids [1,2-dimyristoyl-sn-glycero-3-phosphoethanolamine-N-[methoxy(polyethylene glycol)-2000] (ammonium salt)], purchased through Avanti Lipids and solvated in chloroform. A 270 μL solution of 0.1 % SiNCs in chloroform was put in a 2 mL vial with 200 μL of PEGylated phospholipids in chloroform. Subsequently, 330 μL of chloroform was added while stirring the mixture. Next the mixture was moved into a 50 mL round-bottom flask and attached to Buchi rotary evaporator (R210) set to rotate at 40 rpm for 2-3 hours followed by pulling vacuum of (17 kPa) for 15 minutes to make sure that the solvent was completely evaporated. An image of the setup is shown in figure 6. The flask was removed and hydrated with 2 mL of distilled water and allowed to incubate overnight. During this time, the encapsulation of the SiNCs took place.[4]

The next step is to remove the larger micelles for better contrast and tracking of the small ones. I used two reduction techniques to eliminate undesired large particles. The first

one is by filtration in which we used an Advantec polypropylene in-line filter holder, a Pall hydrophilic polypropylene membrane filter, and a 1 mL syringe. We filtered the micelles through the hydrophilic membrane to get rid of micelles with a size bigger than 200 nm. The second method that I used to separate the small-sized micelles from the large ones is centrifugation in an Eppendorf centrifuge 5424 at a speed of 5000 rpm for 5 minutes.

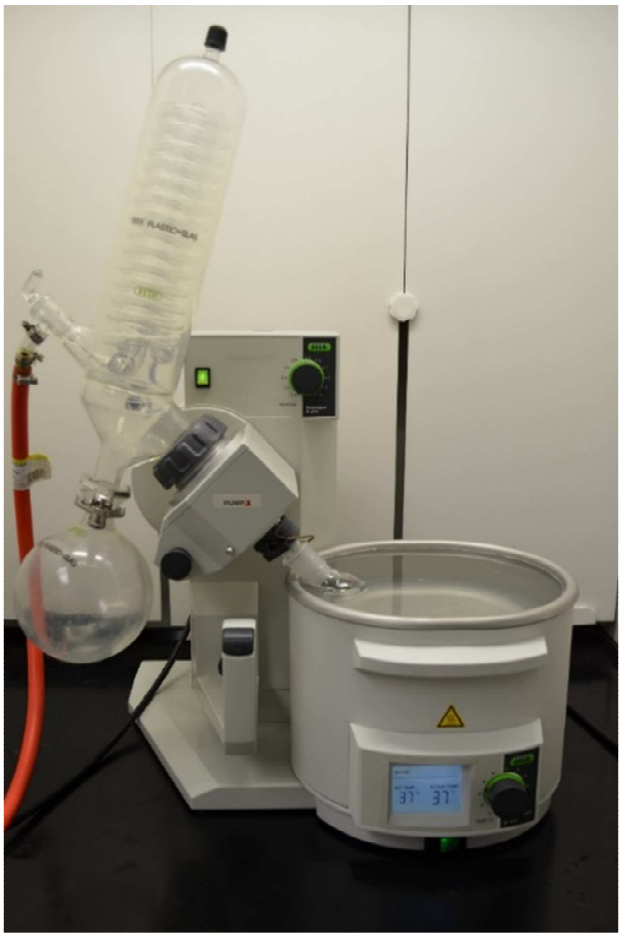

Figure 6: Actual setup for encapsulating SiNCs by PEGylated phospholipids.

The next step is to prepare slides in order to observe the free diffusion of the micelles in water. I cleaned two slides with soap and DI water and dried them under flowing nitrogen to ensure cleanliness. I covered the sides of one slide with a tiny layer of vacuum grease and after putting a drop of the small-sized micelles on the slide, I sandwiched the drop between the two slides. I then have the drop squeezed and sandwiched between the two slides and sealed from air to decrease the evaporation and the movement of the whole drop (Figure 7).

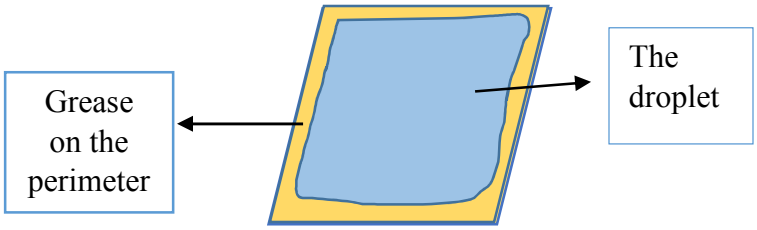

Figure 7: Illustration of how we are preparing the slides to prevent drying.

After preparing the slides, digital movies of the diffusion of the micelles were collected using an inverted Olympus microscope attached to Princeton ProEM Electronic Multiplied Charged Coupled Device (EMCCD). To be able to track the micelles in water *via* their PL, I used an X-Cite® 120Q excitation light source, which uses a 120-watt lamp to deliver rich spectral excitation energy and uniform wide-field fluorescence microscope illumination to the micelles (Figure 8).

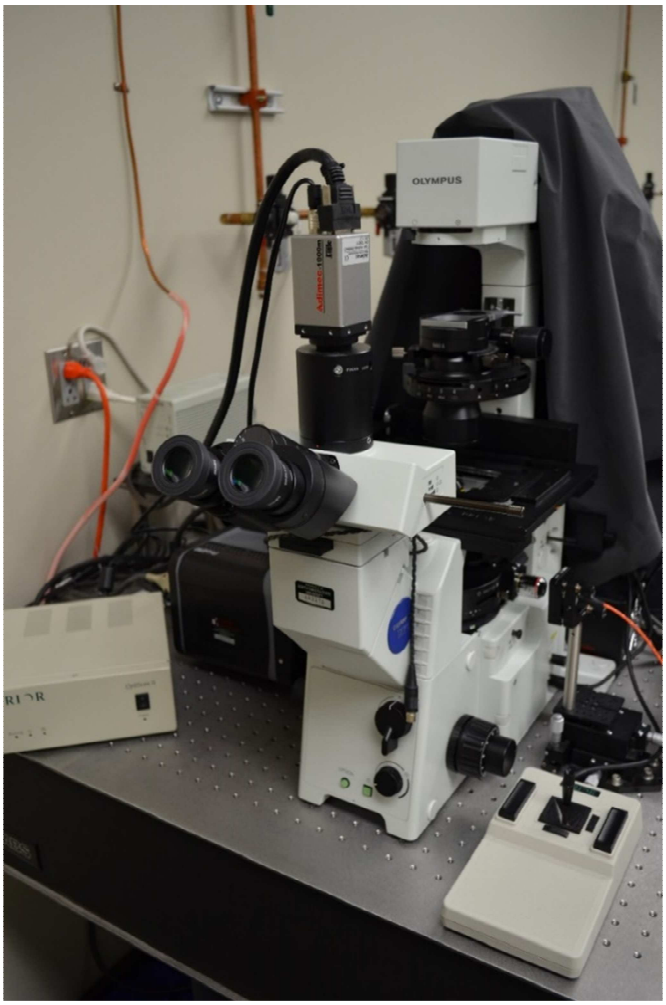

Figure 8: Actual setup of the inverted microscope and epifluorescence method used to collect optical data.

4.2.2. Making Liposomes Using Gentle Hydration Method

After preparing the SiNCs micelles, the next step was to use giant bilayer liposomes as a model for a real biological cellular membrane to examine the interaction between the micelles and the cellular membrane. Liposomes were formed using a 9:1 ratio of (L-α-phosphatidylcholine:L-α-phosphatidylglycerol or PC:PG) lipid mixture in chloroform. Chloroform and methanol were added to achieve a 2:1 (chloroform:methanol) solvent ratio for a total amount of 100 μL in a glass vial. The mixture was hand stirred for five minutes and then put it in a round-bottom tube. The mixture was dried by manual rotation under

the influence of a pure nitrogen flow at a 45-degree angle for 4-5 minutes. I added one to two milliliters of the micelles and then stored the mixture overnight at 37 °C. [21]

The above method that I used to make the liposomes is called gentle hydration. In other studies, the liposomes and micelles are prepared separately then mixed, while we report hydration of the dry layer of lipid mixture with the micelles in water, which allows the liposomes to encapsulate more micelles in a shorter amount of time.

4.2.3. Making of Emulsions

The common emulsion to make is an oil-in-water (O/W) emulsion, where the oil droplets collide in the water environment and are surrounded by surfactant. In our experiment we needed to examine the interaction between SiNC micelles and emulsion walls, so we needed to make a stable water-in-oil (W/O) emulsion. A surfactant or emulsifier is used to surround the water droplets as a shell within the oil environment.[22]

Here, I used sorbitan monostearate (Span® 60) as a surfactant. Span60 has a hydrophilic-lipophilic balance (HLB) of 4.7, which means that it is soluble in oil (or toluene in our case). First, I prepared a solution of 0.5 % of Span60 in 2 mL of toluene and stirred it for 2 minutes by hand until it was totally dissolved. Then, I added 50 μL of our micelles to 500 μL of Span60/toluene solution (10 %). We then stirred it for another 2 minutes and we achieved the desired emulsion.

4.3. Results and Discussion

In this section I report on the three cases of diffusion that I studied. The first is the free diffusion of SiNC micelles in water. The second is the restricted diffusion of SiNC micelles inside GUVs. The third case is the diffusion of SiNCs inside emulsions.

First, I studied the free diffusion of the encapsulated SiNCs in water. I described the recording of digital movies in the previous section. To analyze these videos, I used a Matlab code that we modified (Appendix A). This code was able to track the micelles through each video frame, giving us a data sheet of mean square displacement (MSD) as a function of time. A graph of the MSD versus time for 268 micelles is shown in Figure 8 (left). According to Equation (4.16), we were able to determine the diffusion coefficient values for different micelles as:

$$D = \frac{\langle (r)^2 \rangle}{4t}. \tag{4.16}$$

We could then determine the radius of these micelles using the Stokes-Einstein equation:

$$D = \frac{kT}{6\pi\eta R_h}, \tag{4.17}$$

where $k = 1.38\ X\ 10^{-23}\ m^2 Kg\ s^{-2}K^{-1}$, $T = 300\ K$, η is the viscosity, D is the diffusion coefficient and R_h is the hydrodynamic radius of the micelle.

We determined the viscosity of the solution by calculating it from the previous equation using a micron-sized colloid of known radius by measuring the diffusion coefficient. We calculated the viscosity for two cases: "old" micelles in water solution, with $\eta = 1.156\ mPa,$ and a newer batch in water with $\eta = 1.273\ mPa$. Both values are slightly higher than the viscosity of pure water, which is expected.

From the hydrodynamic size of a large number of such micelles, we then plotted a graph of the normalized photoluminescence intensity, *I*, *vs.* the hydrodynamic radius, R_h (Figure 9).

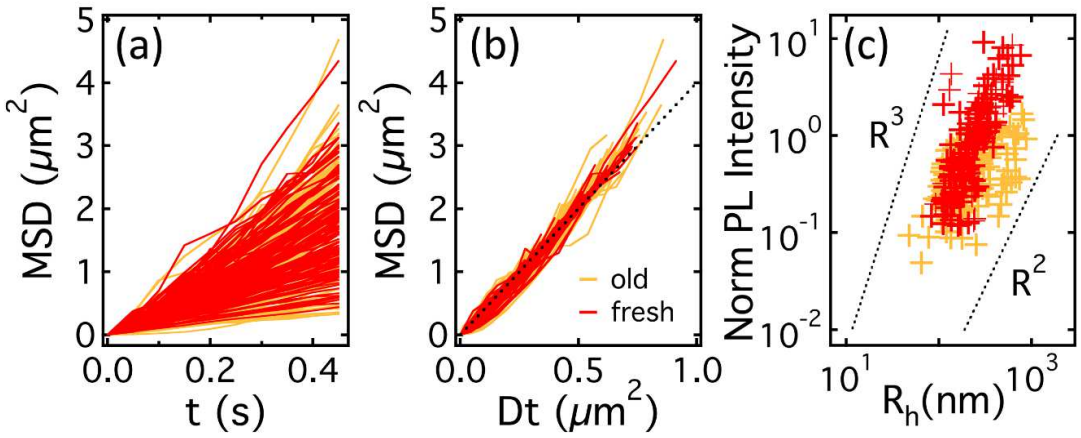

Figure 9: (left) The MSD versus time. (middle) The MSD versus the diffusion coefficient multiplied by time. (right) The normalized photoluminescence intensity versus the hydrodynamic radius.

Second, I studied the diffusion of micelles inside giant unilamellar vesicles (GUVs). After the liposomes encapsulated the micelles, I placed a drop of the solution between two clean slides with grease around the perimeter and started to record movies for the diffusion. Though squeezing of the droplet and surrounding it with grease was helpful in preventing the flow in the whole droplet through drying effects, the liposomes themselves were still moving slowly. This movement was problematic for tracking the micelles so we were not yet able to process all the recorded videos. The liposomes formed in sizes ranging from 5-200 μm. A medium (~ 20 μm) liposome can be seen in the bright field image shown in Figure 11(d). For the liposome videos that we could process, we were able to see the difference between the diffusion of the micelles inside the liposomes and emulsions, which is represented in Figure 10.

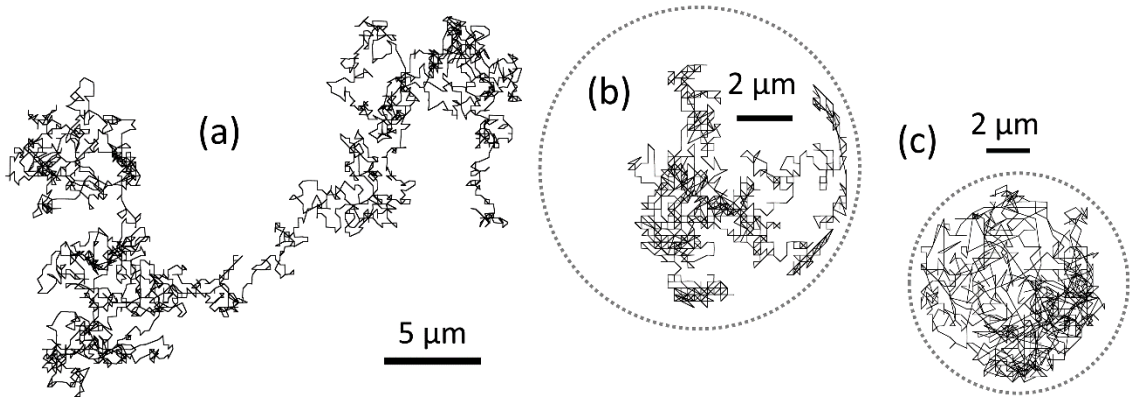

Figure 10: (a) The free diffusion of a micelle in water. (b) The restricted diffusion of a micelle inside an emulsion. (c) The restricted diffusion of a micelle inside a liposome.

Third, I studied the diffusion of micelles inside emulsions as shown in Figure 10(b). I noticed that the movement of the micelles inside emulsions is different from that inside liposomes, as shown in Figure 10(c). Hence, I modified our code to measure the distances between the walls of the emulsion and the micelle and then graphed the data as histograms to study the position probability of the micelles to understand if there is an attractive-potential effect that obligates the micelles to keep moving close to the walls. Although the trajectories suggest that this may indeed be the case, this code is still being refined and such work will not reported in this thesis.

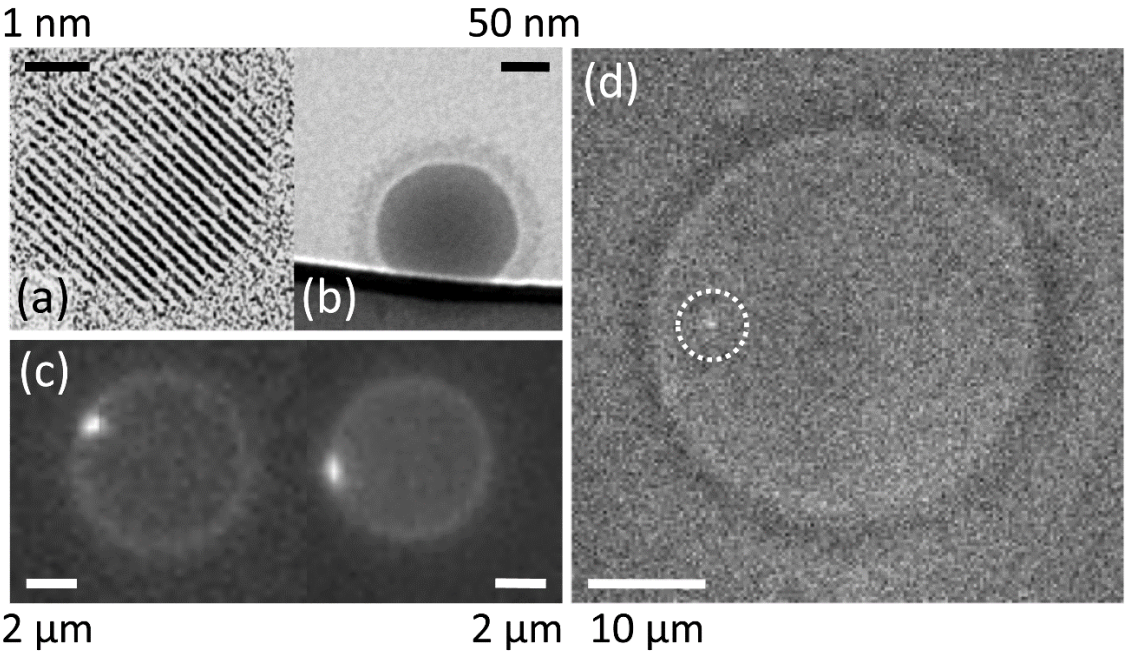

Figure 11: (a) TEM image that shows 1 silicon nanocrystal. (b) TEM image that suggests the QDs are surrounded with polymer ligand (micelle). (c) Images of two different micelles moving along the wall of emulsion. (d) Photo shows micelle moving inside liposome.

4.4. Conclusion

In conclusion, through my work on the diffusion of the micelles in water I determined the hydrodynamic radius for different micelles and found that the photoluminescence intensity scales with the hydrodynamic radius of the micelles. Also, I compared two batches of micelles we made at different times and it showed different trends in intensity, as shown in figure 9. This difference could reflect the effect of water on the micelles because the old batch of the micelles stayed in water longer than the newer one.

The comparison between the data of the micelles inside the liposomes and the emulsions showed a difference in their movement and tendency for the micelles to move beside the walls of emulsions, which is clear by comparing figure 10(b) for a micelle inside an emulsion and figure 10(c) for a micelle inside a liposome. Similar behavior was observed for a large number of micelles in each scenario. Although we suspect that this

difference is due to an attractive potential well around the wall of the emulsion, more investigation is needed to confirm this hypothesis.

REFERENCES

[1] U Kortshagen (2009) Journal of Physics D-Applied Physics 42. Doi:10.1088/0022-3727/42/11/113001

[2] L Brus (1991) Applied Physics a-Materials Science & Processing 53: 465. Doi:10.1007/bf00331535

[3] F Erogbogbo, K-T Yong, I Roy, et al. (2011) Acs Nano 5: 413. Doi:10.1021/nn1018945

[4] F Erogbogbo, KT Yong, I Roy, GX Xu, PN Prasad, MT Swihart (2008) Acs Nano 2: 873. Doi:10.1021/nn700319z

[5] L Pavesi, R Turan (2010) Silicon Nanocystals Fundamentals, synthesis and Applications. WILEY-VCH

[6] K Abderrafi, RG Calzada, MB Gongalsky, et al. (2011) Journal of Physical Chemistry C 115: 5147. Doi:10.1021/jp109400v

[7] CM Hessel, D Reid, MG Panthani, et al. (2012) Chemistry of Materials 24: 393. Doi:10.1021/cm2032866

[8] XG Li, YQ He, MT Swihart (2004) Langmuir 20: 4720. Doi:10.1021/la036219j

[9] X Cheng, R Gondosiswanto, S Ciampi, PJ Reece, JJ Gooding (2012) Chemical Communications 48: 11874. Doi:10.1039/c2cc35954e

[10] M Keidar (2013) Plasma Engineering: Applications from Aerospace to Bio and Nanotechnology. Elsevier,

[11] CR Gorla, S Liang, GS Tompa, WE Mayo, Y Lu (1997) Journal of Vacuum Science & Technology a-Vacuum Surfaces and Films 15: 860. Doi:10.1116/1.580721

[12] G Viera, M Mikikian, E Bertran, PRI Cabarrocas, L Boufendi (2002) Journal of Applied Physics 92: 4684. Doi:10.1063/1.1506382

[13] G Viera, S Huet, M Mikikian, L Boufendi (2002) Thin Solid Films 403: 467. Doi:10.1016/s0040-6090(01)01663-7

[14] MA Lieberman, AJ Lichtenberg (2005) Principles of Plasma Discharges and Materials Processing, 2nd Edition: 1.

[15] YP Raizer (1991) Gas Discharge Physics. Springer, Berlin,

[16] M Hirasawa, T Orii, T Seto (2006) Applied Physics Letters 88. Doi:10.1063/1.2182018

[17] L Mangolini, E Thimsen, U Kortshagen (2005) Nano Letters 5: 655. Doi:10.1021/nl050066y

[18] ML Brongersma, A Polman, KS Min, E Boer, T Tambo, HA Atwater (1998) Applied Physics Letters 72: 2577. Doi:10.1063/1.121423

[19] D Jurbergs, E Rogojina, L Mangolini, U Kortshagen (2006) Applied Physics Letters 88. Doi:10.1063/1.2210788

[20] RAL Jones (2002) Soft Condensed Matter. Oxford University Press,

[21] JP Reeves, RM Dowben (1969) Journal of Cellular Physiology 73: 49. Doi:10.1002/jcp.1040730108

[22] JM Williams (1991) Langmuir 7: 1370. Doi:10.1021/la00055a014

APPENDIX A. MATLAB TRACKING CODE

Some of this Matlab code contains modified programs from [142,143].

PARTICLE TRACKING

```
fname = '2015 April 30 16_55_28_Substack (1-10000)_1.tif';
%info = iminfo(fname);
out = 0;
set = 10; %you can change this according to the number of img in a complete set(number of images that are sequentially tracked correct)
MaxGap = 1.5000; %you can change this according to the max # of imgs that can be fixed.
time = 0.0;
dt = 0.05;
counter = 1;
num_images = 1000;
r2 = 0;
stdev = 19.5;%17.4,18.5,18.2
for k = 1:num_images
   A = imread(fname, k);
   aa = double(A);
   %b=bpass(aa,0,4);
   pk = pkfnd3(aa,18000,11);%*9 & 2 for small
   cnt = cntrd3(aa,pk,2);%2.3333 for smallcomin
   nop = size(cnt);
   numberofparticles=nop(1);

   for l = 1:numberofparticles

   out(counter,4) = time;
```

```
    out(counter,1) = cnt(l,1);
    out(counter,2) = cnt(l,2);
    out(counter,3) = cnt(l,3);
    counter = counter + 1;
    end
    time = time + dt;
end
rows_out = size(out,1);
PredictedOut = out(1,:);

for j = 2:rows_out
    x_j = out(j,1);
    y_j = out(j,2);
    t_j = out(j,4);
    x_jj = out(j-1,1);
    y_jj = out(j-1,2);
    t_jj = out(j-1,4);
    delta_t = round(100*(t_j-t_jj))/100;
    delta_x = x_j - x_jj;
    delta_y = y_j - y_jj;

    if delta_t <= MaxGap
       for m = 1:round(delta_t/dt);
```

```
            Ly = delta_y/delta_t;
            Lx = delta_x/delta_t;
            x_m = x_jj + (Lx*dt*m);
            y_m = y_jj + (Ly*dt*m);
            t_m = t_jj + dt*m;
            V = [x_m y_m -1 t_m];
            PredictedOut = [PredictedOut;V];
        end

    else
        N = out(j,:);
        PredictedOut = [PredictedOut; N];
    end

end
temp = zeros(set,2);
Avg = zeros(set,2);
rows = size(PredictedOut,1);
counter = 0;

%var = 0;
%testVar = zeros(1,2);
```

```
j=0;
for i = 1:rows
        xo = PredictedOut(i,1);
        yo = PredictedOut(i,2);

        if(i+set-1<=rows)

           if i>j
              for j=i+1:i+set-1

                 delta_t = round(100*(PredictedOut(j,4)-PredictedOut(j-1,4)))/100;
                 xj = PredictedOut(j,1);
                 yj = PredictedOut(j,2);

                 if delta_t > MaxGap
                    temp = zeros(set,2);
                    t_j = 0;
                    r2 = 0;
                    xo = PredictedOut(j,1);
                    yo = PredictedOut(j,2);


                 else
```

```
            r2 = ((xj - xo)^2)+((yj - yo)^2);
            temp(j-i+1,1) = j-i;
            temp(j-i+1,2) = r2;

        end
      end
      Avg = Avg+temp;
      %testVar = [testVar;temp];
      temp = zeros(set,2);
      counter = counter + 1;
      %var = [var;j];
    end

  end

end

%RGB = imread('2015 March 26 13_01_42_Substack (1-10000)_Substack (1).png');
%imshow(RGB);

%Rmin = 5;
%Rmax = 200;
```

```
%[center, radius] = imfindcircles(RGB,[Rmin Rmax],'Sensitivity',0.9);

% Display the circle
%viscircles(center,radius);

% Display the calculated center
%hold on;
%plot(center(:,1),center(:,2),'yx','LineWidth',2);
%hold off;

HistogramData = [];
for l = 1:size(PredictedOut,1);
Distance = 97 - (sqrt((111-PredictedOut(l,1))^2 + (113- PredictedOut(l,2))^2));

HistogramData = [HistogramData; Distance];
end


Avg = Avg/counter;


param.mem=6000;
param.dim=2;
```

```
param.good=10;

param.quiet=1;

particles=track(out,100,param);%1.5 for small
```